AIAA JOURNAL
Vol. 44, No. 3, March 2006

Optically Accessible Pressurized Research Combustor for Computational Fluid Dynamics Model Validation

T. Sidwell,* G. Richards,† K. Casleton,‡ D. Straub,§ D. Maloney,¶ P. Strakey,** D. Ferguson,†† S. Beer,‡‡ and S. Woodruff§§
U.S. Department of Energy—National Energy Technology Laboratory, Morgantown, West Virginia 26507

The development of, and results from, the operation of an optically accessible industrial-scale research combustor, designed to provide comprehensive data sets to assist the development of large eddy simulation codes for turbulent combustion applications is discussed. The combustor can be operated at elevated pressure and inlet air temperature, with precisely determined thermal, acoustic, and flow boundary conditions. The effect of fuel composition is investigated by augmenting the natural gas baseline fuel with hydrogen using a lean-premixed combustor configuration. A detailed description of the research combustor and test facility is provided, and recent data on the effects of hydrogen content and combustor heat losses on lean extinction limits, dynamic stability, and pollutant emissions are included. Analysis of the results confirm that heat losses in the combustor play an important role in pollutant formation and that characterization of the thermal boundary conditions is crucial in providing explicit data sets for model validation.

I. Introduction

BECAUSE of their low cost, high efficiency, and favorable environmental performance, gas turbines dominate the market for power generation applications fueled by natural gas. The environmental performance of these systems is the result of advanced combustor designs specifically developed for operation on natural gas fuel. Careful combustor design makes it possible to control many of the chemical reaction pathways that produce criterion pollutants such as NO_X. However, future power plants designed to utilize hydrogen-rich fuels will likely require new combustor designs, or new combustion concepts, to achieve the desired environmental performance and engine reliability.

The shift in baseline fuel composition from natural gas to hydrogen or hydrogen-rich fuels can potentially complicate the development of advanced turbine combustors because combustion-driven dynamics have complicated most commercial attempts to produce natural gas fired low-emission combustors. Problems with dynamics are exacerbated by fuel variability because variations in fuel composition can cause changes in the chemical kinetics and dynamics of the combustion process.[1–3] Fundamental data on the effects of fuel variability on turbulent combustion processes are required to address these problems. Results from the operation of laboratory-scale burners with laminar flames at low pressures and flow rates have been well documented.[4,5] Experimental data at the high-pressure and high-flow operating conditions representative of current industrial-scale gas-turbine combustors, although documented, are less common.[6]

Because of interest in hydrogen and hydrogen-rich fuels for gas-turbine applications, the effects of the fuel variability must be understood before a fuel-flexible combustor can be designed. Increasing the fuel hydrogen content will greatly accelerate the chemical kinetics of the combustion process and the flame speed, which can improve stability at lean conditions and extend operation to leaner conditions.[7] Hydrogen has been studied as an additive to natural gas fuel in gas-turbine applications for NO_X reduction and is of special interest due to the growing popularity of integrated gasification combined cycle (IGCC) power generation systems. In IGCC syngas-based fuels, the hydrogen content of the fuel can vary widely. For example, syngas can be derived from various sources, with fuel hydrogen contents varying from 9 to 62% by fuel volume.[8] This wide fuel composition variation alone is likely to complicate the development process for future gas-turbine combustors and will add significant complexity, time, and cost to the combustor and turbine development process.

Even for gas-turbine systems solely utilizing natural gas fuel, the cost of developing new low-emission turbine combustors is high. A typical development program can last for several years and require repeated hardware testing to resolve unexpected problems with combustion stability, hardware life, and emissions performance. Adapting a low-emission combustor to a fuel with a different composition may require a similar investment, and the high development cost is one factor that prevents routine engine deployment where low emissions are sought on opportunity fuels such as biogas, or hydrogen-rich syngas. Whereas the use of different opportunity fuels would be beneficial for energy production, the cost of developing fuel-specific combustors or redeveloping existing combustors is often too great to justify development for a specific fuel application.

A reliable, low-cost method to evaluate combustor performance during operation with various fuels could greatly reduce the time and cost required to develop these new turbine combustors. Progress in computational fluid dynamics (CFD) modeling of combustion systems has advanced to the point where basic design features are now routinely assessed on the computer. In many instances, these simulations have produced useful qualitative information about the effects of proposed design changes. However, quantitatively accurate prediction of combustion dynamics, pollutant emissions, and the effects of specific fuel chemistry are beyond the capability of current computational models. Technical progress in this area could provide a low-cost method to evaluate the behavior of new fuels in proposed combustor designs.

Received 20 December 2004; revision received 11 May 2005; accepted for publication 31 July 2005.

*Mechanical Engineer, P.O. Box 880, Mail Stop N05, Energy System Dynamics Division; Todd.Sidwell@netl.doe.gov.
†Focus Area Leader, P.O. Box 880, Mail Stop N05, Energy System Dynamics Focus Area. Member AIAA.
‡Physical Scientist, P.O. Box 880, Mail Stop N05, Energy System Dynamics Division.
§Mechanical Engineer, P.O. Box 880, Mail Stop N05, Energy System Dynamics Division.
¶Director, P.O. Box 880, Mail Stop N05, Energy System Dynamics Division.
**Research Scientist, P.O. Box 880, Mail Stop N05, Energy System Dynamics Division.
††Mechanical Engineer, P.O. Box 880, Mail Stop N06, Energy System Dynamics Division.
‡‡Physicist, P.O. Box 880, Mail Stop N05, Energy System Dynamics Division.
§§Research Chemist, P.O. Box 880, Mail Stop N05, Energy System Dynamics Division.

The advancement of computational modeling tools is limited by the availability of experimental data for model development and validation. Central problems in model development include: providing an accurate, computationally tractable representation of key processes in the flame such as turbulence–chemistry interaction subgrid mixing and accurately representing the acoustic, flow, and thermal boundary conditions. In simple laboratory flames, considerable progress has been made on submodel development using experimental data from well-characterized diffusion flames.[9] However, similar data are not available for the type of premixed flames that are used in low-emission turbine combustors. Considerable development efforts have resulted in a variety of methods to model boundary conditions in numerical simulations and to illustrate the significant challenges involved in accurate modeling of these boundary conditions.[10–13]

Because turbine combustors operate at high pressures, with short residence times and high turbulence levels, creating representative test conditions requires specialized facilities. The required pressures and flow rates are typically found only in commercial turbine development labs. These commercial facilities are often occupied with hardware testing for near-term product development, providing limited opportunities to evaluate physical models critical to improved combustion simulations. Experimental data to support modeling efforts for precommercial concepts, such as hydrogen-fueled turbines, are even more difficult to obtain. In these instances, the research payback is too long and speculative to justify investigation by industrial developers, but the need for these data has been highlighted at workshops sponsored by the U.S. Department of Energy.[14,15]

Combustion experiments at the National Energy Technology Laboratory (NETL) conducted as part of the simulation validation (SimVal) studies project are providing comprehensive data sets at operating conditions and scales representative of industrial low-emission turbine combustors. The SimVal combustor is a turbulent, lean-premixed, swirl-stabilized combustor similar in scale to current turbine combustors and is operated at representative pressures, inlet temperatures, and flow rates. Fuel composition variations are investigated by augmenting natural gas fuel with controlled quantities of hydrogen. Optical access to the combustion zone allows observation and characterization of the flowfield. The combustor design provides flexibility to study the effects of changes in combustor geometry, fuel composition, and operating conditions on combustor emissions and dynamics. The boundary conditions are controlled and well quantified. The thermal boundary conditions are determined by measuring the internal and external surface temperatures of the quartz combustor liner with infrared thermometry and by directly measuring the heat losses to the water-cooled metal combustor components. The acoustic boundary conditions are defined by choking the combustor inlet and outlet to isolate the combustor acoustically from upstream and downstream equipment and processes. The inlet flow boundary condition is determined by choking the flow and controlling the turbulent length scales at the nozzle inlet, and the outlet flow boundary condition is determined by choking the flow at the combustor outlet.

Recent data on the effects of hydrogen content and combustor heat losses on lean extinction limits, dynamic stability, and pollutant emissions are presented in this paper. The completed data sets from these experiments ultimately will include detailed boundary condition and flowfield characterization data intended to assist with the development and validation of large eddy simulation (LES) codes for turbulent combustion applications. The complete data sets are available on request, and collaborations with respect to model development and validation are invited.

II. Technical Approach

The SimVal project has been designed to assist the development of LES simulations for advanced gas-turbine combustor applications by producing comprehensive data sets at operating conditions and scales representative of low-emission turbine combustors. The combustor has been designed to provide a computationally tractable geometry and to remove the uncertainties normally present in modeling the boundary conditions, so that model development can focus on accurately modeling turbulence–chemistry interactions and capturing dynamic changes resulting from variations in fuel composition. Combustor operating parameters and geometry can be varied to selectively study their respective effects on combustion mechanisms and performance characteristics such as emissions, dynamics, lean extinction, and flashback. The goal of the current baseline tests was to generate a set of data on the effects of fuel variability that was not complicated by the variation of these geometric and operating parameters. Thus, the combustor was configured to eliminate the mechanisms that drive combustion dynamics. This was primarily accomplished by placing the fuel injection point and mixing region upstream of an inlet choke plate, which decouples this process from the combustion zone. In future studies, the nozzle geometry will be changed from the quiet baseline configuration by progressively changing the fuel injection and inlet choke locations to evaluate systematically how fuel–air mixing affects dynamic mechanisms (Fig. 1). A review of the various mechanisms that drive dynamics has been reported elsewhere.[16,17]

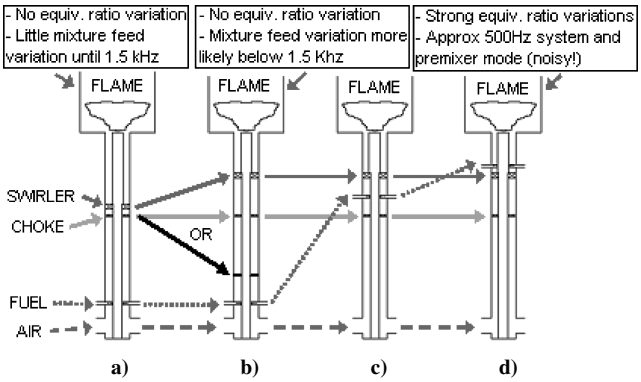

Fig. 1 SimVal combustor nozzle configurations: a) baseline and b–d) future.

The partial data sets produced to date include the following bulk measurements: inlet temperature of the premixed fuel and air (measured in the nozzle); temperature of the products of combustion (measured in the exhaust); combustor pressure (measured at the dump plane); inlet fuel and air volumetric flow rates; heat losses through the cooled metal components and the quartz combustion zone liner; rms pressure (in the nozzle); and emissions. Flowfield data will soon be added to the data sets: Velocity components near the dump plane will be measured by particle image velocimetry (PIV), and the flame structure near the dump plane will be measured by OH planar laser induced fluorescence (OH PLIF), CH chemiluminescence, and OH chemiluminescence.

The test facility consists of the following major components: the optically accessible research combustor; an optically accessible test section; natural gas, hydrogen, and air flow loops; and a gas sample system. In the current test configuration, the facility can provide a maximum combustion airflow rate of 1.23 kg/s, a maximum natural gas flow rate of 53.3 g/s, a maximum hydrogen flow rate of 2.01 g/s, a maximum combustion air preheat temperature of 810 K, and a maximum combustor internal pressure of 2.31 MPa. The geometry of the test section is shown in Fig. 2, and the geometry of the combustor is shown in Fig. 3. Dynamic pressure measurements are made by two high-speed pressure transducers that are spaced axially in the nozzle 10.2 and 15.2 cm upstream of the dump plane. Direct measurement of the exhaust gas temperature can be made with high-temperature thermocouples that are inserted through opposing ports 18.1 and 21.3 cm downstream of the exhaust section inlet. Optical access through the test section is available through four 17.8-cm-wide by 30.5-cm-high viewports. Optical access through the combustor outer liner is available through four equally spaced 10.2-cm-wide by 30.5-cm-high windows that are aligned with the test section viewports. The combustor inner liner is a quartz tube with a length of 31.8 cm and an internal diameter of 18.0 cm, which is representative of the tube diameter of can-style combustors and the dome height of annular combustors. Optical access to the combustion zone allows both direct observation of flame behavior and

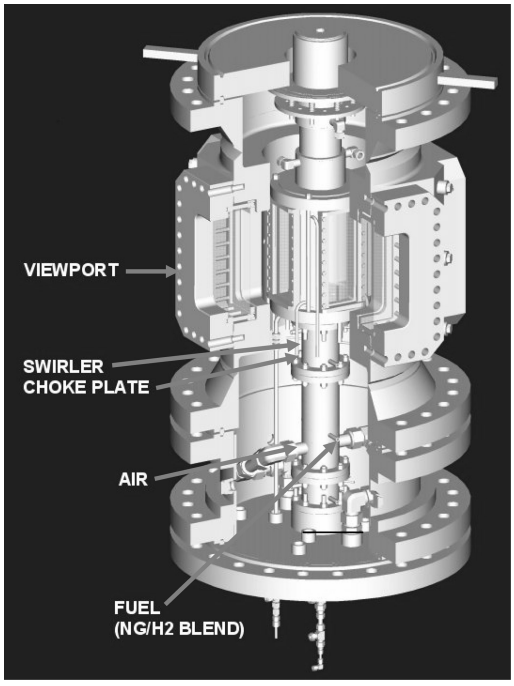

Fig. 2 SimVal test section and combustor configuration.

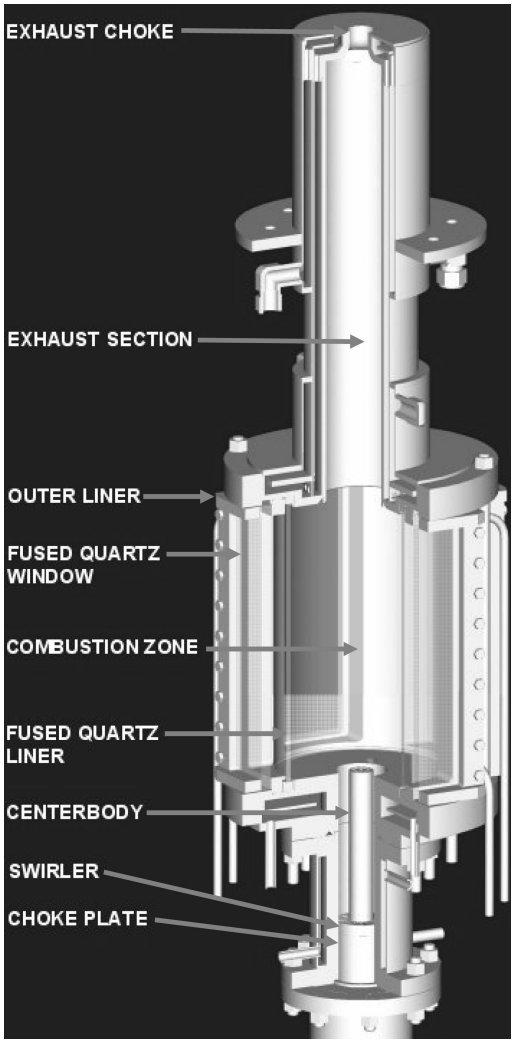

Fig. 3 SimVal combustor baseline configuration.

imaging of the flowfield and flame structure (using OH PLIF, PIV, and CH and OH chemiluminescence) needed to develop physical submodels. OH PLIF measurements have recently been used to measure spatially and temporally resolved reaction rates in turbulent premixed flames.[18] Similar measurements are planned, along with PIV, to provide a combined measure of velocity and scalar quantities with the goal of improving submodel descriptions of the reacting flowfield. A full description of the combustor geometry and test conditions can be acquired by contacting the lead author.

To prepare for measurement of the velocity field in hot, reacting flows at elevated pressures, cold-flow, atmospheric-pressure PIV measurements of the velocity field at the dump plane of a geometrically equivalent combustor were performed at NETL. The inlet airflow rates were scaled to provide nozzle velocities of approximately 50 m/s to match the nozzle velocities of the hot-flow, pressurized tests conducted to date. Alumina particulate with a nominal diameter of 1 μm was used as the seed material, and a Nd:YAG laser was used to generate the laser sheet. High-quality images were produced with image areas varying between 34 and 125 mm square. Full results from these tests will be reported at a later date in a separate paper.

Obtaining flowfield characterization data from this full-scale combustor will provide important data for both model development and model validation. However, by using just these diagnostic techniques, many of the fundamental features of the local reaction zone cannot be observed. In turbine combustors, the reacting flow length and timescales cover a broad range from centimeters to micrometers, and milliseconds to nanoseconds. Because experimental resolution of the smallest of these time and length scales is difficult, conditional moment statistics between velocity and scalar quantities will be used to infer events occurring at these scales. Obtaining these data, even in laboratory flames, represents the frontier of combustion diagnostics. To capitalize on the data produced in these experiments, NETL is collaborating with external research groups such as the Sandia National Laboratory Combustion Research Facility to perform these advanced measurements.

It is possible that the quality of the data to be obtained by each optical diagnostic method could be limited by either the combustor geometry, that is, field of view, or the combustor operating conditions, that is, elevated pressure. Elevated operating pressures are not expected to have a significant negative effect on the data collected with the planned diagnostic methods, but the extent of any negative effect will not be known until data are actually collected. Imaging of the flowfield may be limited to the 10.2-cm width of the combustor outer liner windows, depending on the position and field of view of the imaging camera, but even this minimum width would still allow the velocity components and flow structure at the nozzle dump plane to be imaged. The current outer liner configuration will prevent imaging with PIV and OH-PLIF within 3 mm of the combustor dump plane. This gap may be reduced practically to 1 mm with relatively minor modifications to the outer liner. The fused quartz viewport windows and combustion liner are expected to reduce transmitted laser power and signal intensity during the planned OH PLIF and PIV measurements. These losses have been characterized and are likely to require only reduced imaging areas to provide acceptable image signal-to-noise ratios. The resolution of neither the flowfield characterization data nor the OH and CH chemiluminescence data is expected to be reduced significantly.

Collection of data with OH PLIF and PIV is currently limited to planar (two-dimensional) data. Thus, PIV images of the velocity field will be limited to two simultaneous velocity components in the plane of the laser sheet. A vertical laser sheet coincident with the combustor centerline will provide axial and radial velocity components, whereas a horizontal laser sheet parallel to the dump plane will provide radial and tangential velocity components.

Independent or combined application of additional laser diagnostic methods such as Raman and Rayleigh scattering have been applied in turbulent combustion processes to yield useful localized species concentration and temperature data.[19] Future implementation of localized diagnostic methods such as these is possible, but due to the complexities that would be introduced by these methods,

they will not be implemented presently. Aside from the complexities arising directly from implementation of the diagnostics, it is likely that the viewport windows at the pressure boundary would need to be redesigned due to the concentrated laser energy required by these methods and to assure sufficient signal strength and data quality. Thus, laser diagnostics will initially be limited to planar laser diagnostic methods such as the aforementioned PIV and OH-PLIF methods.

A. Flow Boundary Conditions

In the baseline configuration, the combustor inlet is designed to provide an upstream flow boundary condition that results in a fully premixed fuel–air mixture and acoustically isolates the combustion processes from upstream processes and hardware. A 12.7-mm-thick slot swirler (Fig. 4) is set in the nozzle annulus 17.1 cm upstream of the combustor dump plane. The slot swirler was designed to control the wake and separation regions to the flow, as is inevitable with conventional vane swirlers. Accurate simulations must account for these detailed flow features, which range from the small wake originating at the vane trailing edge to the large eddies that may be shed from separation bubbles, particularly during transients. For the purposes of gathering baseline validation data, it is desirable to reduce or avoid this disparity in flow scales. The slot swirler contains radial slots that are angled at 30 deg with respect to the flow axis and are spaced to produce approximately equal wake and flowpaths, with dimensions that are small enough so that the nonuniformity in the flow will dissipate before arriving at the flame front.

It has been suggested that the small size of the slots will allow for a numerical description of the boundary without needing a fine grid in the nozzle region, that is, the individual slots may not need to be resolved to provide an accurate description of the inlet flow conditions at the dump plane, at least in the context of steady Reynolds-averaged Navier–Stokes (RANS) calculations. RANS-based CFD simulations of the nonreacting flowfield in the nozzle section of the baseline configuration were performed during the design process and indicated that the flow nonuniformities would indeed dissipate in the nozzle before reaching the dump plane. Whereas truncation of the experimental domain to simplify the modeling domain may be useful for steady-state RANS calculations in the absence of acoustics, it is expected that unsteady simulations such as LES will need to include the nozzle section, at least as far as the swirler, to provide more physically realistic boundary conditions. This will alleviate the need to prescribe artificial acoustic boundary conditions such as nonreflecting mass flow inlets and pressure outlets. Also, the turbulent flowfield generated by the swirler would, thus, be implicitly treated in the simulation, rather than being prescribed as a boundary condition. Although this does increase the size of the computational domain somewhat, it is believed that the rigor of this approach will be necessary to capture the more elusive combustion phenomenon such as unsteadiness and thermoacoustic coupling.

Whereas the slot swirler is expected to be a valuable feature for model development, a test of model predictions must ultimately include a conventional swirl vane geometry. Tests with a conventional flat-vane swirler will be conducted after the baseline tests are completed. In addition to providing simulation validation data, a comparison of the combustor performance with these two swirler configurations will demonstrate the importance of the inlet flow boundary conditions on low-emission combustion. For example, the irregular vortices shed from large vanes may play a role in destabilizing combustors operating at the edge of lean extinction. It is expected that data collected in the SimVal tests will show this effect, which could then be used to enhance new combustor extinction limits.

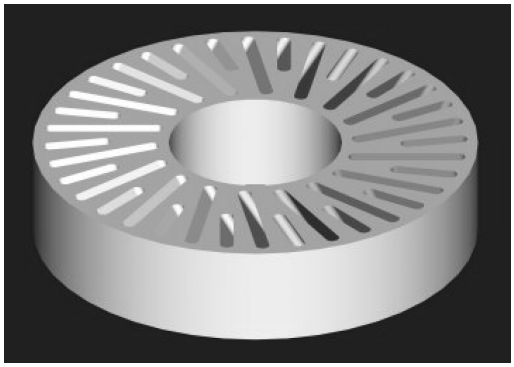

Fig. 4 SimVal combustor slot swirler for baseline configuration.

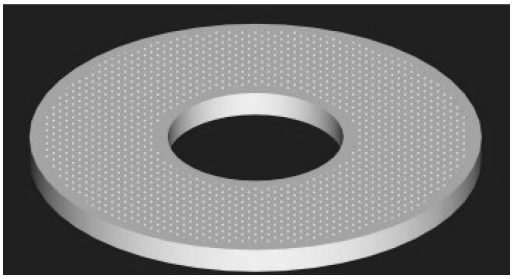

Fig. 5 SimVal combustor inlet choke plate.

The approach flow supplied to the swirler should, ideally, be uniform. This is accomplished in the current combustor configuration by installing an inlet choke plate (Fig. 5) 12.7 mm upstream of the leading face of the swirler. The plate chokes the flow of premixed fuel and air by restricting the flow to ∼1320 laser-drilled, 0.43-mm holes that are evenly distributed across the annulus. In this baseline configuration (and unlike a conventional fuel–air premixer) fuel is injected into the combustion airstream upstream of the swirler through eight radial fuel injection spokes that are arrayed in a single plane 25.7 cm upstream of the inlet choke plate. This approach produces a spatially uniform flow immediately above the choke plane, isolates the flow acoustically from upstream processes and hardware, and assures full premixing of the fuel–air mixture. When fuel is injected upstream of the inlet choke plate, the complication of describing fuel–air mixing is intentionally avoided. However, the level of premixing will affect both dynamics and emissions[20] and, therefore, must be addressed experimentally. The combustor will be reconfigured in future tests to inject fuel downstream of the inlet choke plate to study the effects of mixing on combustion dynamics and pollutant formation.

B. Acoustic Boundary Conditions

To describe combustion dynamics, the acoustic impedance of all of the boundaries must be known. Because the combustor uses no dilution or cooling jets, the solid walls of the combustor can all be treated as acoustically hard. Although it has been shown that wall compliance, that is, vibration, in practical combustion liners can produce an acoustic response in the combustion chamber,[21] this effect is small in practical devices and is negligible in the SimVal combustor where the walls are cooled and are not compliant. Thus, the only boundary conditions of acoustic interest are the exit and inlet.

The exit boundary is a choked orifice at the end of the exhaust section that is designed to isolate the combustor acoustically from downstream processes and hardware. This type of boundary has been extensively studied in rocket combustion acoustics[22] and can be described easily in numerical simulations. The inlet boundary serves as both a flow and acoustic boundary, and care must be taken to produce a flow that is uniform in space and constant in time. A simple choked orifice will not provide these conditions because the high-speed flow would need to decelerate in a diffuser located before the swirl vanes. As pressure waves move toward the choke, they would enter regions of progressively larger Mach numbers and would gradually reflect off of both the diffuser walls and the flow. The result is a fairly compliant boundary, requiring a diffuser long enough to develop a uniform flow. This requirement is undesirable for these tests because the added diffuser length would set the impedance of the fuel nozzle at levels that are so low that it would be difficult to avoid low-frequency oscillations at many operating conditions. This behavior has been affirmed experimentally in unpublished tests at NETL. In addition to providing a uniform inlet flow distribution as described earlier, the inlet choke plate also

provides a hard acoustic boundary condition. The orifice sizes are sufficiently small so that each orifice functions as a choke point, and flow diffusion occurs very close to the orifice exit, producing a spatially uniform flow immediately above the choke point but retaining the needed choke condition.

A choked orifice is located at the end of the exhaust section, which is a resonant section with a 50.8-cm length and 9.0-cm diameter. The resonant section is sized to produce a primary resonant mode near 500 Hz, a frequency of interest in fielded gas-turbine engines. A second resonant mode near 1400 Hz may also be excited, but frequencies in the kilohertz range are less common in typical stationary turbine combustors. The geometry of the resonant exhaust section can be modified to produce responses at other frequencies without appreciably modifying the flowfield in the combustor.

The effects of any bulk variation in the fuel–air composition entering the combustor were minimized by selecting the length of the exhaust section to avoid matching the nozzle and combustor acoustic modes and to create high impedance where the nozzle empties into the dome. The fuel–air variation[23] that often couples with dynamics was avoided by premixing the fuel and air upstream of the choke plate. It was also recognized that fluid mechanical disturbances originating at the swirler could lead to heat release variation through a change in the flame area.[24] This mechanism was minimized by placing the swirler just 12.7 mm above the choke plate, ensuring that the swirler was located at a position of very high acoustic impedance. In this manner, pressure perturbations arriving at the vanes would produce minimal changes in the acoustic velocity. The results presented in this paper will show that the incorporated design features were effective at avoiding dynamic instability in the baseline configuration and that no thermoacoustic oscillations were observed over the range of test conditions and fuel composition studied.

Additional nozzle configurations will be tested to study the mechanisms that contribute to thermoacoustics in engine applications. In practical situations, additional complications will arise from irregular fuel–air premixing. The inlet boundary will have a much different acoustic impedance because practical fuel injectors are not choked. In most engine configurations, the inlet boundary communicates acoustically with the plenum fed by the compressor discharge, so that the acoustic impedance is determined by the geometry of both the compressor discharge region and the fuel injector itself.

Because the acoustic arrangement of the compressor discharge is engine specific, there is no single preferred geometry for this aspect of the test program. Instead, the most beneficial data would be produced by reporting the effect of both low- and high-impedance cases. This will be achieved in future tests by relocating the acoustic choke from its location in the baseline configuration. The baseline configuration in Fig. 1a has relatively high impedance until frequencies above 1.5 kHz. For those frequencies, so-called mixture-feed instabilities are possible. In this situation, a one-quarter wave resonance in the premixer passage can produce substantial fluctuations in the total mixture supplied to the flame. Frequencies in this range are less common in fielded engines, although they do occur. Based on the results of tests previously conducted at NETL,[20] these high-frequency oscillations are expected to be confined to specific portions of the operating map and should be a useful test of the prediction capability of numeric simulations.

In Fig. 1b, the swirler is moved downstream in the nozzle, increasing the possibility that vortices shed from the swirler will interact with and cause instabilities at the flame front. This mechanism would most likely be observed with the replacement of the slot swirler with a conventional swirl vane. In a variation of the configuration shown in Fig. 1b, the choke point is moved upstream in the nozzle. This configuration produces a low nozzle impedance around 500 Hz, close to the natural frequency of the combustor–resonator assembly. Quarter-wave resonance in the premixer will again produce mixture feed instabilities, but in this configuration the 500-Hz frequencies are more typical of fielded engines. Unlike fielded engines, this arrangement will still use completely premixed fuel and air. These data will, therefore, provide a test for numeric simulations that still avoids uncertainties of premixing fuel and air, but captures the dynamic features of oscillations at frequencies that are relative to real applications.

In the configurations shown in Figs. 1c and 1d, the fuel is injected downstream of the choke plate and is injected either upstream or downstream of the swirler. These configurations include all of the relevant physics of a low-emission combustor, but include well-defined boundary conditions. By gradually adding physical complexity in the test (moving from Fig. 1a to Fig. 1d), data for simulation validation can be tested in progressively complex steps. This approach will ensure that inadequacies in physical submodels can be identified in isolation, rather than being obscured by the effects of the multiple mechanisms that will be present in the final configuration in Fig. 1d.

C. Thermal Boundary Conditions

The thermal boundary conditions at the walls of a combustion chamber can play a major role in determining the performance of the final device because combustion dynamics can be complicated by hysteresis loops resulting from the temperature of the combustor walls.[25] The metal-walled sections of the combustor, the nozzle, centerbody, dome, outer liner, and exhaust section, are backside water cooled to allow quantification of heat losses and provide close estimates of the combustor wall temperatures. Although the resulting wall temperatures are lower than in actual engine applications, the value of the experiment for producing model validation data is not compromised because the cooling scheme virtually removes the ambiguity of the thermal boundary conditions at the metal surfaces.

To measure the temperature distributions on the inside and outside surfaces of the quartz combustion zone liner, the liner is marked with black high-temperature paint stripes that are oriented axially and circumferentially on the inner and outer surfaces of the tube. The infrared emissions from these paint stripes during operation are recorded using a charge-coupled device camera and an 800-nm infrared (IR) filter and are correlated to the inner and outer wall temperatures, providing temperature and partial heat transfer boundary conditions. Figure 6 shows representative liner temperature measurements and the paint stripe orientation.

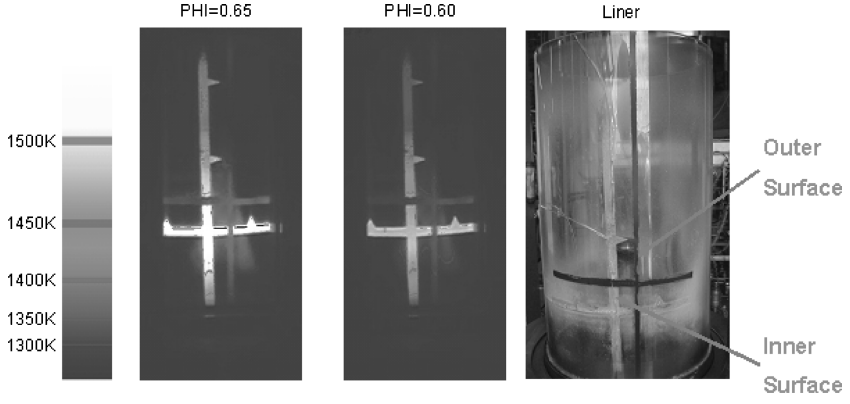

Fig. 6 Liner thermal images and paint stripe orientation.

Calibrations were performed with a commercial blackbody source at 14 temperature settings from 1133 to 1463 K to determine the effective wavelength (778 nm) of the filter/camera assembly. Subsequent single-point blackbody calibrations were taken at 1463 K, using the effective wavelength to calculate paint strip temperatures. Effective paint strip emissivities, including transmission losses through the quartz liner and optical access window, were determined from the reflection coefficients for intact portions of the paint strips after the run. These emissivities were 0.7 and 0.8 for the interior and exterior strips, respectively. Uncertainties in the differences between the inside and outside wall temperatures is estimated at 20 K, due largely to temperature gradients within the strips and variation in the paint emissivities during testing.

D. Emissions Measurement

Emissions measurements are made by continuous sampling from the exhaust stream just downstream of the choked orifice at the end of the combustor exhaust. A portion of the heated gas sample passes through an NO_2-to-NO converter to prevent the loss of water soluble NO_2 in the chiller/dryer that reduces water content to less than 1% by volume. This gas stream provides sample to the NO_X and O_2 analyzers. The NO_X analyzer has a full-scale range of 0–20 ppm (vol) with an accuracy of 1% full scale. The remainder of the gas sample, which flows through a separate leg of the chiller/dryer, is analyzed by a mass spectrometer for CO_2, O_2, Ar, H_2O, and N_2 content and by individual analyzers for CO, CO_2, and unburned hydrocarbon content.

These emissions measurements provide a valuable measure of the ability of CFD codes to predict accurately overall combustion performance. Because the predictive capabilities of CFD codes with respect to bulk emissions are dependent on their prediction of turbulence–chemistry interactions, the level of agreement between computationally predicted and experimentally measured emissions is a good initial estimate of the prediction of these interactions. At certain operating conditions, minimal changes in operating conditions can cause sudden changes in combustor acoustics and abrupt and significant changes in bulk emissions. These abrupt transitions in acoustics and emissions can be captured experimentally and provide a measure of the ability of CFD codes to predict the underlying thermoacoustic interactions. The diagnostic methods to be utilized for flowfield characterization described earlier in this section will provide more detailed data on localized flame structures and phenomena to allow further, localized evaluation of the predictive capabilities of the codes.

III. Test Procedure

Baseline tests using natural gas and natural gas/hydrogen fuel mixtures to evaluate pollutant emissions, lean extinction, and dynamics (Table 1) were conducted at combustion air flow rates of 0.26 and 0.38 kg/s, which correspond to combustor operating pressures of 0.43 and 0.63 MPa respectively. All tests were conducted using fully premixed fuel and air, with no pilot fuel added during testing. Hydrogen was added to the natural gas fuel to produce four fuel compositions for each combustion airflow rate: 0, 10, 20, and 40% hydrogen (by total fuel volume) at an airflow rate of 0.26 kg/s, and 0, 5, 10, and 20% hydrogen (by total fuel volume) at an airflow rate of 0.38 kg/s. While holding the combustion airflow rate and fuel composition (hydrogen percentage) constant, the fuel flow rates were gradually decreased over the course of the test until significant flame fluctuations near lean extinction and a significant increase in the rms pressure were observed. These criteria were based on experience from tests to lean extinction and were expected to produce a ramp endpoint within 0.01 of the equivalence ratio at lean extinction. Lean extinction was approached but was intentionally avoided to prevent damage to the quartz combustor liner. To determine the presence of hysteresis effects, the fuel flow rates then were increased gradually until the original flow rates were reached.

Additional tests were performed to gather data at lean extinction. Again, these tests were conducted using fully premixed fuel and air and were conducted at a combustion airflow rate of 0.38 kg/s. Hydrogen was added to the natural gas fuel to produce fuel compositions of 5 and 10% (by total fuel volume). While holding the combustion airflow rate and fuel composition (hydrogen percentage) constant, the fuel flow rates were gradually decreased until lean extinction.

IV. Results

Emissions data collected during operation of the research combustor are presented in Fig. 7. The NO_X data are corrected to an exhaust O_2 content of 15% by volume and are effectively on a dry basis. Note that the residual moisture content of the gas samples reaching the analyzers does not exceed 0.6% by volume and is typically 0.3% or less by volume.

In Fig. 7, NO_X emissions are shown to decrease smoothly with equivalence ratio. The absence of discontinuities in the equivalence ratio sweeps is consistent with having only minimal combustion dynamics or variations in fuel composition. The addition of hydrogen to the natural gas fuel, even in small quantities, significantly decreases the lean extinction limit and extends the envelope of stable operations to much leaner equivalence ratios. At these leaner operating conditions, NO_X emissions can be decreased due to lower flame temperatures and decreased thermal NO_X formation. Additional moisture that would be generated from the presence of hydrogen in the fuel has been shown in studies of humidified air turbine cycles to reduce significantly NO_X by both thermal as well as nonthermal routes.[26]

The slight increase in NO_X levels with increasing combustor pressure observed in Fig. 7 is attributed to an increase in combustor temperature with operating pressure. As the operating pressure (and mass flow rate) of the combustor is increased, the inlet air temperature also increases as a result of decreased heat loss in the feed lines. Also, the heat losses in the combustor (when expressed as a total percentage of the heating value of the fuel) decrease with increasing pressure, because the heat transfer does not scale linearly with the mass flow rate and pressure.

Table 1 Planned test conditions

Air flow rate, kg/s	Combustor pressure, MPa	Air preheat temperature, K	H_2 content, %	Equivalence ratio	Ramp time, min
0.26	0.43	550	0	$0.59 \rightarrow 0.51 \rightarrow 0.59$	60
0.26	0.43	550	10	$0.53 \rightarrow 0.45 \rightarrow 0.53$	60
0.26	0.43	550	20	$0.53 \rightarrow 0.45 \rightarrow 0.53$	60
0.26	0.43	550	40	$0.53 \rightarrow 0.45 \rightarrow 0.53$	60
0.38	0.63	550	0	$0.59 \rightarrow 0.51 \rightarrow 0.59$	60
0.38	0.63	550	5	$0.53 \rightarrow 0.45 \rightarrow 0.53$	60
0.38	0.63	550	10	$0.53 \rightarrow 0.45 \rightarrow 0.53$	60
0.38	0.63	550	20	$0.53 \rightarrow 0.45 \rightarrow 0.53$	60
0.38	0.63	550	0	$0.53 \rightarrow 0.44$ (No test)	30
0.38	0.63	550	5	$0.53 \rightarrow 0.44$ (To lean extinction)	30
0.38	0.63	550	10	$0.53 \rightarrow 0.44$ (To lean extinction)	30

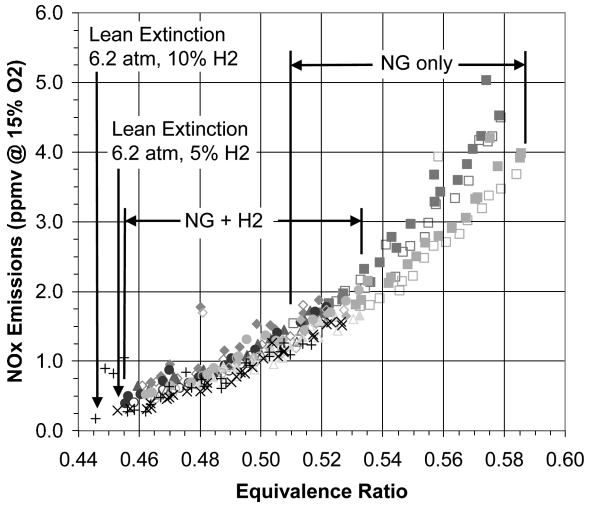

Fig. 7 NO_X (corrected to 15% O_2) vs equivalence ratio for natural gas with and without H_2 addition: ■, 6.2 atm, 0% H_2 (down); □, 6.2 atm, 0% H_2 (up); ◆, 6.2 atm, 5% H_2 (down); ◇, 6.2 atm, 5% H_2 (up); ▲, 6.2 atm, 10% H_2 (down); △, 6.2 atm, 10% H_2 (up); ●, 6.2 atm, 20% H_2 (down); ○, 6.2 atm, 20% H_2 (up); ■, 4.2 atm, 0% H_2 (down); □, 4.2 atm, 0% H_2 (up); ◆, 4.2 atm, 10% H_2 (down); ◇, 4.2 atm, 10% H_2 (up); ▲, 4.2 atm, 20% H_2 (down); △, 4.2 atm, 20% H_2 (up); ●, 4.2 atm, 40% H_2 (down); ○, 4.2 atm, 40% H_2 (up); ×, 6.2 atm, 5% H_2 (lean extinction); and +, 6.2 atm, 10% H_2 (lean extinction).

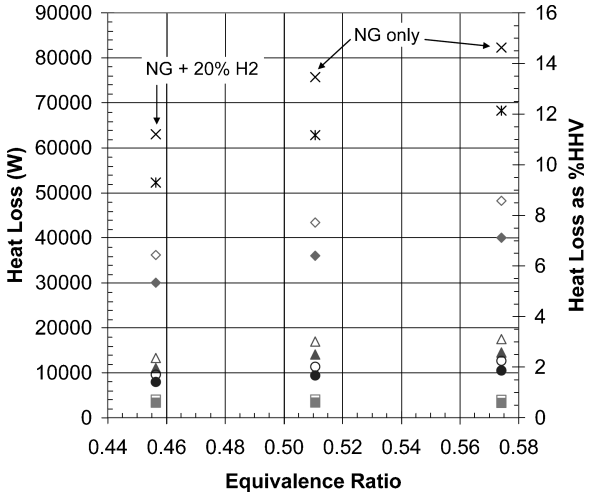

Fig. 8 Heat losses (total and percomponent) vs equivalence ratio: ▲, nozzle and dome; ■, centerbody; ●, liner metal; ◆, liner quartz; ✳, total; ×, % higher heating value (HHV) total; ◇, % HHV liner quartz; ○, % HHV liner metal; □, % HHV centerbody; and △, % HHV nozzle and dome.

Heat losses from the combustion zone at lean conditions are expected to have an especially significant effect on emissions, dynamics, and flame stability limits. This research combustor is expected to produce greater heat losses than those from typical commercial combustors, due specifically to the backside water cooling of the metal components and the radiant heat losses through the quartz combustor liner. Figure 8 shows heat losses (in watts and as a percentage of fuel higher heating value) as a function of equivalence ratio. However, the effects of the heat losses are expected to be partially offset by the absence of liner cooling airflow typical of industrial combustors. The heat losses are expected to have an effect on the emissions, dynamics, and flame stability for a given operating condition, and the heat losses are quantified in these tests, allowing for interpretation of the data.

In Fig. 9, NO_X emissions are plotted against adiabatic and nonadiabatic flame temperatures and illustrate the effects of heat losses on emissions and flame temperature. NO_X emissions are plotted against adiabatic flame temperatures in the rightmost data group-

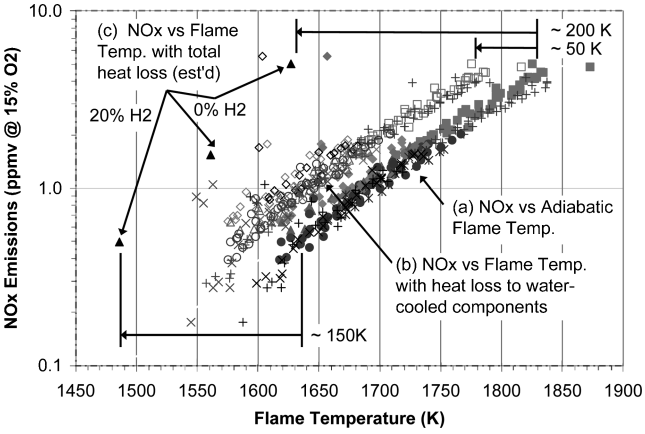

Fig. 9 NO_X (corrected to 15% O_2) vs flame temperature (adiabatic and nonadiabatic) for natural gas with and without H_2 addition.

ing. The adiabatic flame temperatures are derived from equilibrium calculations using Cantera[27] and Chemkin[28] software with the GRI-Mech 3.0 mechanism.[29] These calculations are performed with the measured fuel and airflow rates and the measured premix fuel and air temperature and pressure. When heat losses to the cooled metal combustor components (the centerbody, nozzle, dome, and outer liner) are added to the flame temperature calculations, the NO_X data are shifted approximately 50 K from the adiabatic flame temperature. This difference in flame temperature is the result of radiant and convective heat losses to the centerbody, nozzle, and dome and radiant heat losses to the outer liner. The heat losses in the quartz combustor section are estimated using the wall temperature measured with the IR camera and are the combined effects of convection and radiation from the combustion gas to the quartz liner, radiation from the combustion gas through the quartz liner to the surroundings, and radiation from the quartz liner to the surroundings. When the total heat losses from the quartz combustion zone and the exhaust section are taken into account, the NO_X data are shifted approximately 150–200 K from the adiabatic flame temperature. The difference in the flame temperature for these data points is the result of the total heat loss from the combustor, which adds the measured heat loss to the exhaust section.

The flame temperature calculations used to represent the data points in Fig. 9 use the measured peak liner surface temperatures, estimated temperatures of the combustor surroundings, estimated bulk properties for the combustion gas, and estimated bulk properties for the combustion liner. The heat transfer calculations are currently based on empirical correlations[30] and are calculated conservatively to provide a lower bound on the flame temperature decrease due to the total heat loss.

Figure 9 shows an initial, first-order estimate of the effects of reactor heat loss on NO_X formation and demonstrates the importance of defining the thermal boundary conditions. In an effort to quantify the coupled effects of temperature, mixing, and kinetic timescales on pollutant formation, a series of CFD simulations of the SimVal combustor were performed using the commercial CFD code Fluent. A nominal operating condition of 4.1 atm and an equivalence ratio of 0.6 for natural gas and air at an inlet temperature of 530 K were selected as a test case. The two-dimensional axisymmetric computational domain consisted of approximately 5000 grid cells with a velocity inlet boundary located at 5 cm upstream of the dump plane. Separate three-dimensional unreacting computations were performed for the nozzle section to estimate the inlet velocity and turbulence profiles for the two-dimensional reacting calculations. A pressure outlet boundary was used at the exhaust choke.

The turbulence model used for the steady-state RANS calculations performed here was the renormalized group theory model with a modification for highly swirling flows. RANS calculations were suitable in this case because the conditions being modeled were steady. In cases where dynamics are expected, LES

calculations would be required. The turbulence chemistry interaction was modeled with the eddy dissipation concept proposed by Magnussen.[31] The reaction mechanism employed here was a 15 step, 19 species augmented reduced mechanism (ARM) developed for lean-premixed methane–air combustion.[32] This particular ARM is a skeletal reaction mechanism reduced from the full GRI-Mech 3.0 reaction set. The ARM is a computer optimized reaction mechanism that is designed to reproduce NO and CO formation using a reduced chemistry set that includes NO formation from the Zeldovich, Fenimore, and N_2O pathways.

Two simulation cases are presented here. The first is with adiabatic wall boundary conditions. The second case employs wall boundary conditions derived from the measured SimVal heat fluxes, as well as a radiation model to account for radiation from the combustion gas to (and through) the quartz liner, as well as the metal components of the combustor. Figure 10 is a comparison of static temperature contours for the two cases. The inlet boundary is on the left of Fig. 10 and the pressure outlet on the right. The bottoms of Figs. 10a and 10b represent the axisymmetric boundary, whereas the tops represent the walls of the combustor. The flame location and shape, which is primarily the white region in the contour plots, is in good qualitative agreement with observed flame shape in the experiments. The slightly hotter temperature in the corner of the combustor for the adiabatic case (Fig. 10a) is due to the recirculation zone located here that provides increased residence time for CO burnout to CO_2. Figure 10 shows the significant temperature difference between the adiabatic and nonadiabatic case. The reactor exit temperatures were 1842 and 1545 K for the adiabatic and nonadiabatic cases, respectively, which is a difference of almost 300 K.

Figure 11 shows a comparison of NO mole fractions for the two cases. The NO mole fractions were roughly twice as high for the adiabatic case and appear to be primarily a function of the peak flame temperature in the quartz reactor section that is affected by radiative losses, as well as convective recirculation of cooler gas near the liner wall back into the flame zone, thus, reducing the peak flame temperatures for the nonadiabatic case. The NO mole fractions at the reactor exit were 12.1 and 5.9 ppm for the adiabatic and nonadiabatic cases, respectively. The experimentally measured NO mole fraction for this case was 7.8 ppm.

Figure 12 shows a comparison of CO mole fractions for the two cases. The white areas on the contour plots are regions where the CO mole fraction was in excess of 50 ppm. The adiabatic case (Fig. 12a) resulted in nearly twice as much CO being produced in the flame region, which was similar to the NO results. A much larger effect is, however, observed in the exhaust section where the adiabatic case results in very little CO burnout with an exit mole fraction of 34.8 ppm. The cooling of the exhaust gas in the nonadiabatic case results in much greater conversion of the CO to CO_2 with an exit CO mole fraction of only 4.5 ppm, which is much closer to the experimentally observed CO mole fraction of about 4 ppm for this case. The results of the simulations presented in Figs. 11 and 12 clearly demonstrate the importance of characterizing the thermal boundary conditions for providing model validation data because the chemical kinetics are extremely sensitive to heat losses and gas temperature.

The experimentally measured dynamic behavior of the combustor is shown in Fig. 13. As mentioned earlier, combustion dynamics in these tests have been prevented by careful design and configuration of the combustor. Geometric changes planned for later tests are likely to promote dynamics. In Fig. 13, the combustor rms pressure is normalized against the mean combustor pressure and is plotted vs equivalence ratio. The rms pressure levels are very low over most of the operating range and increase only at the lean extinction limit.

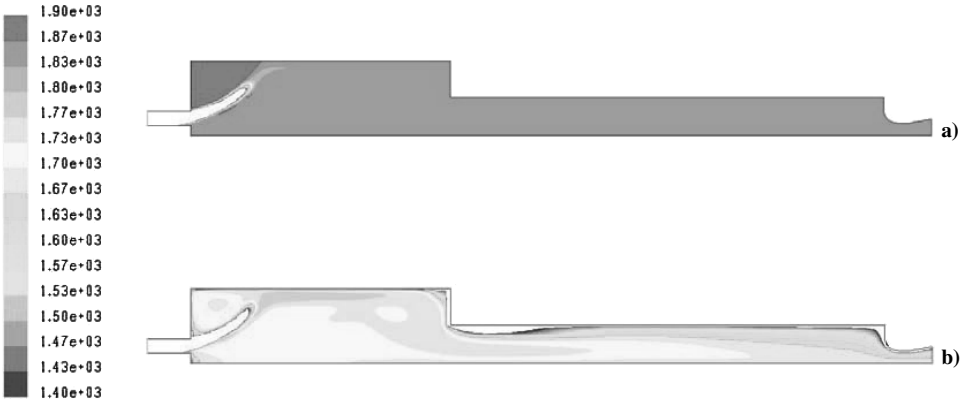

Fig. 10 Temperature contours (1400–1900 K) from CFD simulations for a) adiabatic and b) nonadiabatic case.

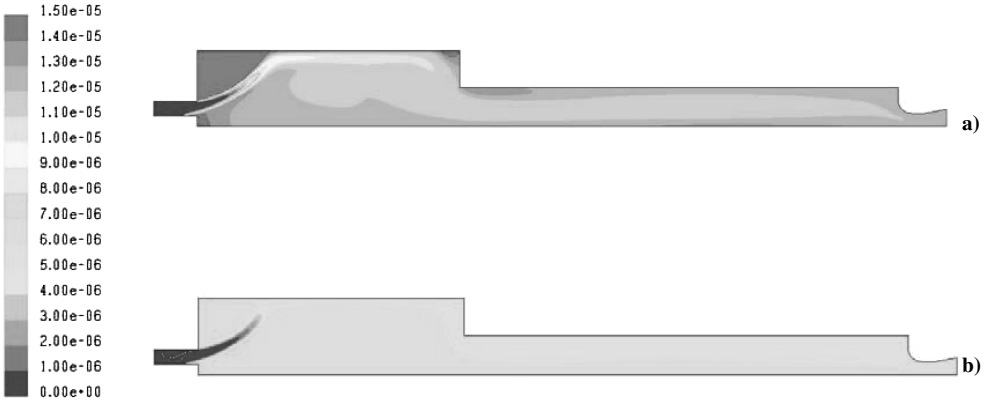

Fig. 11 NO mole fraction contours (0–15 ppm) from CFD simulations for a) adiabatic and b) nonadiabatic case.

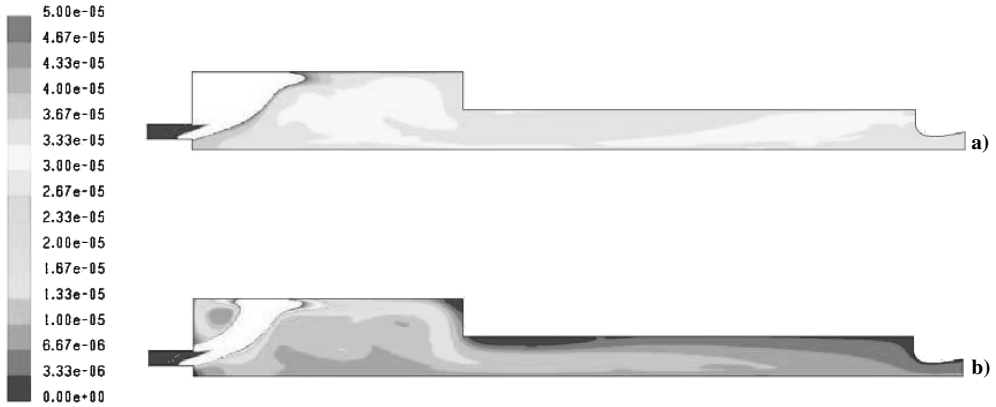

Fig. 12 CO mole fraction contours (0–50 ppm) from CFD simulations for a) adiabatic and b) nonadiabatic case.

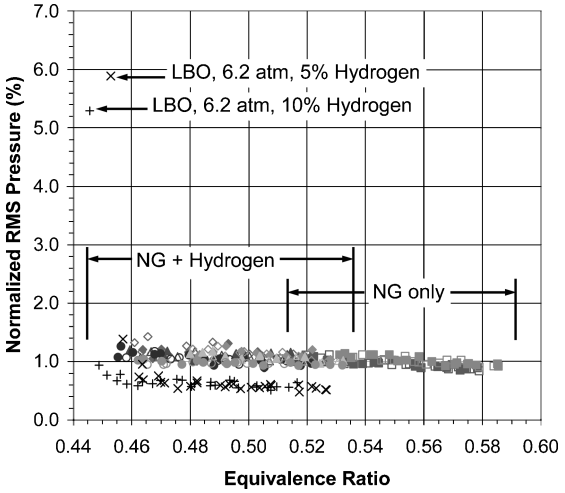

Fig. 13 RMS pressure (normalized to mean combustor pressure) vs equivalence ratio for natural gas with and without H_2 addition: ■, 6.2 atm, 0% H_2 (down); □, 6.2 atm, 0% H_2 (up); ◆, 6.2 atm, 5% H_2 (down); ◇, 6.2 atm, 5% H_2 (up); ▲, 6.2 atm, 10% H_2 (down); △, 6.2 atm, 10% H_2 (up); ●, 6.2 atm, 20% H_2 (down); ○, 6.2 atm, 20% H_2 (up); ■, 4.2 atm, 0% H_2 (down); □, 4.2 atm, 0% H_2 (up); ◆, 4.2 atm, 10% H_2 (down); ◇, 4.2 atm, 10% H_2 (up); ▲, 4.2 atm, 20% H_2 (down); △, 4.2 atm, 20% H_2 (up); ●, 4.2 atm, 40% H_2 (down); ○, 4.2 atm, 40% H_2 (up); ×, 6.2 atm, 5% H_2 (lean extinction); and +, 6.2 atm, 10% H_2 (lean extinction).

V. Conclusions

The research combustor described in this paper provides data on the effects of fuel variability and heat losses on lean extinction limits, dynamic stability, and pollutant emissions at conditions representative of low-emission turbine combustors. The combustor is designed to provide flexibility in studying the effects of changes in combustor geometry, fuel composition, and operating conditions (temperatures, pressures, and flow rates), with precisely determined thermal, acoustic, and flow boundary conditions.

The results of the experiments conducted to date agree with previous results that show that the addition of hydrogen to natural gas fuel, even in small quantities, decreases the lean extinction limit and extends stable operation to lower equivalence ratios than are possible with natural gas alone. Combustion dynamics were prevented in these tests due to the configuration of the combustor in its baseline, acoustically quiet configuration. The results of CFD simulations demonstrated the importance of well-defined thermal boundary conditions with respect to pollutant formation.

The completed data sets from this continuing series of experiments ultimately will include boundary condition and flowfield characterization data, and are intended to assist the development and validation of numeric simulations for turbulent combustion applications. The partial data sets produced to date include the following bulk measurements: inlet temperature of the premixed fuel and air, exhaust temperature of the products of combustion, combustor pressure, inlet fuel and air volumetric flow rates, heat loss through the cooled metal components and the quartz combustion zone liner, combustor rms pressure; and emissions. Upcoming experiments will provide detailed flowfield measurements for generating validation data for CFD models with an emphasis on LES codes and submodels. Flowfield data will include PIV measurements of the velocity components near the dump plane, and OH PLIF, CH chemiluminescence, and OH chemiluminescence images of the flame structure near the dump plane. Geometric changes and fuel composition effects that are expected to promote the appearance of combustion dynamics (and characteristic, abrupt transitions in performance measures such as emissions) for specific operating conditions will be studied. The data sets are available on request, and collaborations with respect to simulation development and validation are welcome.

Acknowledgments

This work was sponsored by the U.S. Department of Energy Turbines Program. The support of both past and current Technology Managers, Abbie Layne and Richard Dennis, is gratefully recognized. The authors thank Mark Tucker, Thaddeus Dera, Michael Bierer, and Justin May for their efforts in assembling, maintaining, and operating the test facility and Clinton Bedick for his assistance with flame temperature calculations.

References

[1]Janus, M. C., Richards, G. A., Yip, M. J., and Robey, E. H., "Effects of Ambient Conditions and Fuel Composition on Combustion Stability," American Society of Mechanical Engineers, Paper 97-GT-266, June 1997.

[2]Scholz, M. H. H., and DePietro, S. M., "Field-Experience on DLN Typhoon Industrial Gas Turbine," American Society of Mechanical Engineers, Paper 97-GT-061, June 1997.

[3]Nord, L. O., and Andersen, H. G., "A Study of Parameters Affecting the Combustion Stability and Emissions Behavior of Alstom Heavy-Duty Gas Turbines," American Society of Mechanical Engineers, Paper GT2004-53228, June 2004.

[4]Alavandi, S. K., and Agrawal, A. K., "Lean Premixed Combustion of Methane and Hydrogen-Enriched Methane Using Porous Inert Media," American Society of Mechanical Engineers, Paper GT2004-53231, June 2004.

[5]Wicksall, D. M., Agrawal, A. K., Schefer, R. W., and Keller, J. O., "Fuel Composition Effects on the Velocity Field in a Lean Premixed Swirl-Stabilized Combustor," American Society of Mechanical Engineers, Paper GT2003-38712, June 2003.

[6]Griebel, P., Scharen, R., Siewart, P., Bombach, R., Inauen, A., and Kreutner, W., "Flow Field and Structure of Turbulent High-Pressure Premixed Methane/Air Flames," American Society of Mechanical Engineers, Paper GT2003-38398, June 2003.

[7]Phillips, J. N., and Roby, R. J., "Enhanced Gas Turbine Combustor Performance Using H2-Enriched Natural Gas," American Society of Mechanical Engineers, Paper 99-GT-115, June 1999.

[8]Todd, D. M., "Gas Turbine Improvements Enhance IGCC Viability," *Gasification Technologies Conference 2000*, Gasification Technologies Council, Arlington, VA, 2000.

[9]Mbiock, A., Barlow, R., and Roekaerts, D. (eds.), *The 5th International Workshop on Measurements and Computation of Turbulent Nonpremixed Flames*, Sandia National Labs., Livermore, CA, 2000, pp. 18–235.

[10]Grinstein, F. F., Young, T. R., Gutmark, E. J., Li, G., Hsiao, G., and Mongia, H. C., "Flow Dynamics in a Swirl Combustor," *Journal of Turbulence*, Vol. 3, No. 030, 2002, pp. 1–19.

[11]Grinstein, F. F. (ed.), "Special Section on 'Boundary Conditions for Large Eddy Simulation,"' *AIAA Journal*, Vol. 42, No. 3, 2004, pp. 437–492.

[12]Baum, M., Poinsot, T., and Thevenin, D., "Accurate Boundary Conditions for Multicomponent Reactive Flows," *Journal of Computational Physics*, Vol. 116, No. 2, 1994, pp. 247–261.

[13]Poinsot, T., and Veynante, D., *Theoretical and Numerical Combustion*, R.T. Edwards, Philadelphia, 2001, pp. 409–450.

[14]Arellano, L., and Smith, K., "Combustion Activities and Research Needs," *AGTSR Combustion Workshop VII*, South Carolina Inst. for Energy Studies, Clemson, SC, 2000.

[15]Rosfjord, T., and Proscia, W., "Technology Needs for Low Emission, Industrial Gas Turbines," *AGTSR Combustion Workshop VII*, South Carolina Inst. for Energy Studies, Clemson, SC, 2000.

[16]Richards, G. A., Straub, D. L., and Robey, E. H., "Passive Control of Combustion Dynamics in Stationary Gas Turbine Combustors," *Journal of Propulsion and Power*, Vol. 19, No. 5, 2003, pp. 795–810.

[17]Mongia, H. C., Held, T. J., Hsiao, G. C., and Pandalai, R. P., "Challenges and Progress in Controlling Dynamics in Gas Turbine Combustors," *Journal of Propulsion and Power*, Vol. 19, No. 5, 2003, pp. 822–829.

[18]Lee, S.-Y., Seo, S., Broda, J. C., Pal, S., and Santoro, R. J., "An Experimental Estimation of Mean Reaction Rate and Flame Structure During Combustion Instability in a Lean Premixed Gas Turbine Combustor," *Proceedings of the Combustion Institute*, Vol. 28, Pt. 1, No. 1, 2000, pp. 775–782.

[19]Masri, A. R., Dibble, R. W., and Barlow, R. S., "The Structure of Turbulent Nonpremixed Flames Revealed by Raman–Rayleigh–LIF Measurements," *Progress in Energy and Combustion Science*, Vol. 22, No. 4, 1996, pp. 307–362.

[20]Shih, W., Lee, J., and Santavicca, D. A., "Stability and Emission Characteristics of a Lean Premixed Gas Turbine Combustor," *The Twenty-Sixth Symposium (International) on Combustion*, Combustion Inst., Pittsburgh, PA, 1996, pp. 2771–2778.

[21]Cronemyr, P. J., Hulme, C. J., and Troger, C., "Coupled Acoustic-Structural Analysis of an Annular DLE Combustor," American Society of Mechanical Engineers, Paper 98-GT-502, June 1998.

[22]Zinn, B. T., Bell, W. A., Daniel, B. R., and Smith, A. J., Jr., "Experimental Determination of Three-Dimensional Liquid Rocket Nozzle Admittances," *AIAA Journal*, Vol. 11, No. 3, 1973, pp. 267–272.

[23]Steele, R. C., Cowell, L. H., Cannon, S. M., and Smith, C. E., "Passive Control of Combustion Instability in Lean Premixed Combustors," *Journal of Engineering for Gas Turbines and Power*, Vol. 122, No. 3, 2000, pp. 412–419.

[24]Kunze, K., Hirsch, C., and Sattelmayer, T., "Transfer Function Measurements on a Swirl Stabilized Premix Burner in an Annular Combustion Chamber," American Society of Mechanical Engineers, Paper GT2004-53106, June 2004.

[25]Straub, D. L., and Richards, G. A., "Effect of Nozzle Configuration on Premix Combustion Dynamics," American Society of Mechanical Engineers, Paper 98-GT-492, June 1998.

[26]Bhargava, A., Colket, M., Sowa, W., Casleton, K., and Maloney, D., "An Experimental and Modeling Study of Humid Air Premixed Flames," *Journal of Engineering for Gas Turbines and Power*, Vol. 122, No. 3, 2000, pp. 405–411.

[27]Goodwin, D. G., "An Open-Source, Extensible Software Suite for CVD Process Simulation," *Chemical Vapor Deposition XVI and EUROCVD 14*, Electrochemical Society, Pennington, NJ, 2003.

[28]Kee, R. J., Rupley, R. M., Meeks, E., and Miller, J. A., "Chemkin-III: A FORTRAN Chemical Kinetics Package for the Analysis of Gas-Phase Chemical and Plasma Kinetics," Sandia National Labs., Technical Rept. SAND96-8216, Livermore, CA, May 1996.

[29]Smith, G. P., Golden, D. M., Frenklach, M., Moriarty, N. W., Eiteneer, B., Goldenberg, M., Bowman, C. T., Hanson, R. K., Song, S., Gardiner, W. C., Jr., Lissianski, V. V., and Qin, Z., "GRI-Mech 3.0," Univ. of California, Berkeley, CA, URL: http://www.me.berkeley.edu/gri_mech/ [cited 19 January 2006].

[30]Lefebvre, A. H., *Gas Turbine Combustion*, Taylor and Francis, Philadelphia, 1999, pp. 275–285.

[31]Magnussen, B. F., "On the Structure of Turbulence and a Generalized Eddy Dissipation Concept for Chemical Reaction in Turbulent Flows," AIAA Paper 81-42, Jan. 1981.

[32]Sung, C. J., Law, C. K., and Chen, J. Y., "Augmented Reduced Mechanisms for NO Emission in Methane Oxidation," *Combustion and Flame*, Vol. 125, No. 1–2, 2001, pp. 906–919.

F. Grinstein
Guest Editor